# Nanostructured Hybrid Solar Cells: Dependence of the Open Circuit Voltage on the Interfacial Composition

By *Neil D. Treat, Luis M. Campos, Michael D. Dimitriou, Biwu Ma, Michael L. Chabinyc,** and *Craig J. Hawker**

Inverted polymer solar cells[1,2] fabricated using transparent metal oxide cathodes have received significant attention due to their potential for improved lifetime and performance compared to conventionally structured organic solar cells.[3] An additional attractive feature of this design is that low temperature, solution processed metal oxides can be employed allowing for compatibility with plastic substrates.[4] We have used soft imprint lithography to pattern solution-processable amorphous titanium sub-oxide ($a$-$TiO_x$) and to examine the effect of electrode surface area and active layer processing procedures on performance of bulk heterojunctions (BHJs) of poly(3-hexylthiophene) (P3HT) and [6,6]-phenyl-C61-butyric acid methyl ester (PCBM). Increasing the electrode surface area of the diodes noticeably improved the charge injection in forward bias, but had little effect on charge extraction. The open circuit voltage, $V_{oc}$, was sensitive to both the electrode geometry and processing method, suggesting a non-uniform morphology for the BHJ in the nanopores, which impacts the open circuit voltage.

Affordable production of the state-of-the-art silicon-based photovoltaics is limited by a need for large-area silicon substrates with low electronic defect densities.[5] Thin-film organic photovoltaics (OPVs) offer the potential to be fabricated at low cost over virtually any size substrate due to their solution processability.[6] OPVs have achieved power conversion efficiencies of near 8%, which is close to the estimated efficiencies of 10% needed to achieve economic viability,[6,7] and are currently limited by their coverage of the solar spectrum[8] and by optoelectronic loss processes in the cells.[7,9] Significant effort has been directed towards improving their efficiency through the synthesis of new materials[7] and by the development of a fundamental understanding the nature of charge carrier generation and loss.[10]

One strategy to improve the stability and performance of BHJ OPVs is to form cells with an inverted structure. In inverted cells, wide band gap semiconductors are used to form the cathode rather than a low work function metal. Typically, these inverted devices use transparent, conducting oxide cathode materials such as $TiO_2$[1,11] and ZnO[12] that can be deposited by sputtering or using sol-gel precursors followed by high temperature (>200 °C) calcination. An alternate approach that is compatible with plastic substrates involves the use of a low temperature, solvent-processable amorphous electron transporting material.[1,2] Simultaneous hydrolysis and polycondensation (in ambient conditions) of an organometallic precursor yields an amorphous titania layer, $a$-$TiO_x$, at low temperatures (≈100 °C).[13]

Ordered heterojunctions involving nanoscale patterning of the metal oxide materials have recently gained significant attention due to their precise control over the spatial arrangement of the donor and acceptor domains. The development of robust and patternable materials have allowed soft nanoimprint lithography (SNIL) to become an attractive route towards nanostructured solar cells.[15] This strategy allows for the preservation of the master through the fabrication of polymeric stamps that can be used multiple times to fabricate nanopatterned substrates.[14] McGehee and coworkers have described the fabrication of a calcined nanostructured $TiO_2$ with a P3HT donor phase,[15] however this system is plagued by low short circuit current due to inefficient charge separation at the $TiO_2$/P3HT interface. In order to more efficiently harvest excitons, we report the fabrication of nanoporous $a$-$TiO_x$ using poly(3-mercaptopropylmethylsiloxane) stamps[16] and infiltration of these structures with a P3HT:PCBM blend.

SNIL was used to fabricate cathodes of $a$-$TiO_x$ with a surface area that is nearly three times greater than that of a conventionally structured electrode (details on the characterization of $a$-$TiO_x$ are found in the Supporting Information). A combination of poly[(3-mercaptopropyl)methylsiloxane] and multifunctional crosslinking materials was used to prepare the patterned stamp by the previously published procedure, using a porous aluminum oxide template (pore diameter and height of 50 nm and 150 nm respectively).[14] The nanostructured $a$-$TiO_x$ substrates were fabricated and characterized by cross-section SEM and found to have pore dimensions of approximately 60 nm in diameter and 70 nm in depth (**Figure 1**). It should be noted that the resulting pores are both wider and shallower than the inverse structure of the stamp because of shrinkage during curing.[17] The active layer, composed of a 1:0.7 mixture by weight of P3HT:PCBM and 2 vol% of 1,8 octanedithiol, was subsequently spin coated on the nanopatterned substrates. The as-cast films were observed to rest on top of the nanopattern (see Supporting Information, Figure S1), thus subsequent processing steps were required to achieve full infiltration and

[*] N. D. Treat, Dr. L. M. Campos, M. D. Dimitriou, Prof. M. L. Chabinyc, Prof. C. J. Hawker
Materials Research Laboratory
Materials Department
Mitsubishi Chemical Center for Advanced Materials
University of California Santa Barbara
Santa Barbara, CA 93106 (USA)
E-mail: mchabinyc@engineering.ucsb.edu; hawker@mrl.ucsb.edu
Dr. B. Ma
The Molecular Foundry
Lawrence Berkeley National Laboratory
Berkeley, CA 94720 (USA)

DOI: 10.1002/adma.201001967

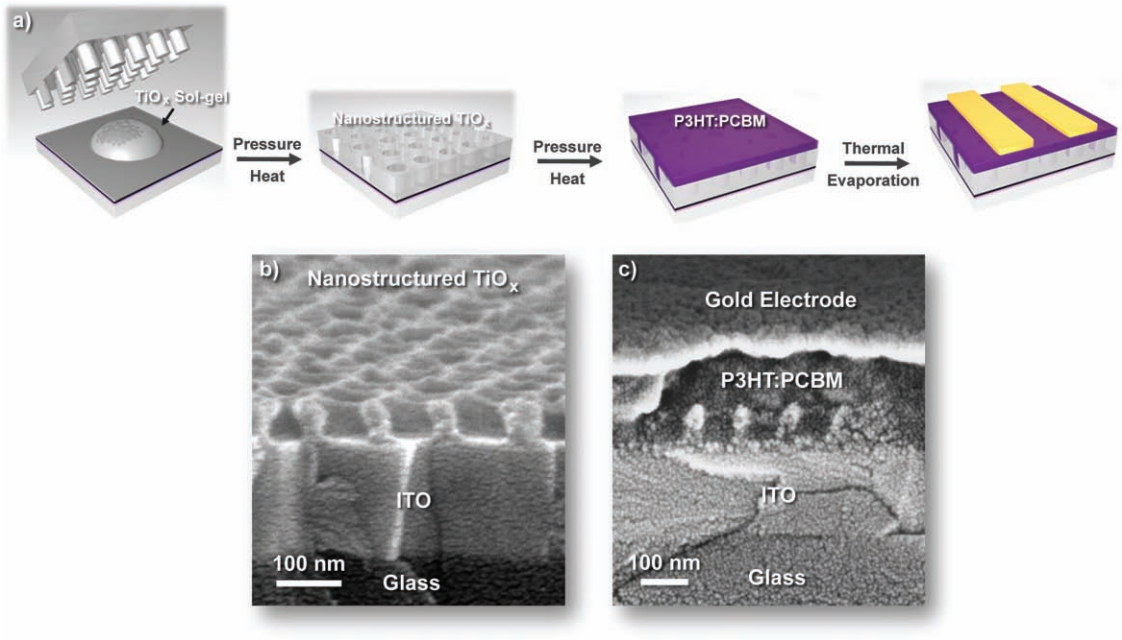


**Figure 1.** a) Schematic representation of the fabrication of nanopatterned $TiO_x$ solar cells, b) cross-section SEM of nanopatterned *a*-$TiO_x$ (60 nm wide × 70 nm deep), and c) cross-section SEM of the final nanopatterned device (glass/ITO/*a*-$TiO_x$/P3HT:PCBM/Au).

interfacial contact. Optimal results were achieved by using a flat soft stamp fabricated from the materials described above and applying pressure (approximately 300 psi) and heating at 150 °C for 30 min in an argon atmosphere. Gold anodes were then deposited via thermal evaporation (Figure 1c). The flat and nanopatterned *a*-$TiO_x$ devices had nearly the same volume of active layer material (within 3% measured by the thicknesses of the as-processed films). Furthermore, there was no observed difference in the UV-vis transmission absorption and external quantum efficiency.

Solar cells with nanopatterened and flat thin-film *a*-$TiO_x$ cathodes were fabricated to compare the impact of electrode geometry on optoelectronic performance. A xenon arc lamp equiped with a solar filter was used to provide the AM 1.5G spectra at 100 mW $cm^{-2}$. It should be noted that the series resistance of cells containing *a*-$TiO_x$ as the cathode material were sensitive to the illumination time and the UV content of the solar spectrum.[4,18] In this study, the devices were light soaked at zero bias for a minimum of 5 min to minimize this effect (see Supporting Information). A summary of the median efficiencies for P3HT and P3HT:PCBM active layers, electrode geometries, and active layer processing can be found in the Supporting Information (Table S1). The nanopatterend *a*-$TiO_x$ devices had a best efficiency of 1.47% and a median of 1.03%. Typical device performances were achieved by spin coating a 17 mg $mL^{-1}$ solution (based on polymer concentration) of P3HT:PCBM (1:0.7 by wt) with 2% vol 1,8 octanedithiol at 1100 rpm. It should be noted that these devices were never exposed to air, which has been shown to reduce the open-circuit voltage ($V_{oc}$) and thus, the device performance.[4] Finally, solar cells with a conventional geometry were fabricated using the same active layer materials and thicknesses used in the inverted cells in this study and were found to give consistent efficiencies of ≈3% (see the Supporting Information).

In the *a*-$TiO_x$/BHJ solar cells, there are effectively three heterojunctions, P3HT/*a*-$TiO_x$, PCBM/*a*-$TiO_x$, and P3HT/PCBM. Efficient charge generation is not expected from the PCBM/*a*-$TiO_x$ heterojunction interface due to the similar energies of the lowest unoccupied molecular orbital (LUMO) and conduction band. However, both the P3HT/*a*-$TiO_x$ and the P3HT/PCBM interfaces can dissociate excitons. If the P3HT/*a*-$TiO_x$ heterojunction were efficient at generating charge, then the short circuit current, $J_{sc}$, would likely scale with the surface area of the *a*-$TiO_x$ interface. However, it was observed that the $J_{sc}$ did not scale relative to the electrode surface area indicating charge separation occurs mainly at the P3HT/PCBM interface (**Figure 2a**).[1] The increase in cathode surface area lead to higher currents in forward bias than planar devices. Contributions from the difference in dielectric constants of P3HT, PCBM, and *a*-$TiO_x$ to the electric field in these devices should only have a small effect on the mobility of the material; due to the aspect ratio, the charge density at the pore wall is increased in a small fraction of the layer and thus has little effect on the device performance.[19]

The most significant difference between the device characteristics of the flat and nanopatterned cathodes was the increase in $V_{oc}$ of the nanopatterned devices by 0.1 V relative to the thin-film devices.[20] The $V_{oc}$ in organic solar cells is a property of the active layer materials and the electrodes, therefore it is surprising that changes in the electrode geometry could increase the $V_{oc}$. Furthermore, based on the conventional model of photovoltaics (a current generator in parallel with a diode), the larger forward bias current of the nanopatterned *a*-$TiO_x$ devices would likely lead to a decrease in $V_{oc}$

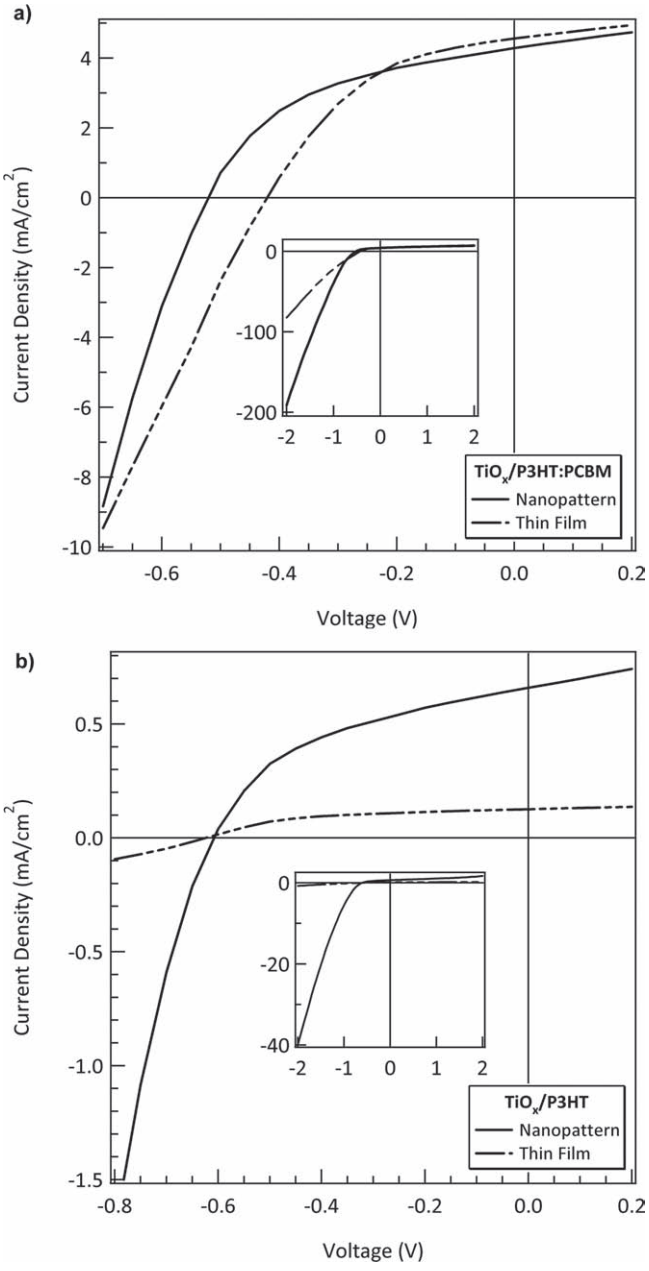


**Figure 2.** Current–voltage curves for nanopatterned (60 nm diameter × 70 nm deep) and thin-film a) *a*-$TiO_x$/P3HT:PCBM devices processed with heat and pressure and b) *a*-$TiO_x$/P3HT devices processed with heat and pressure. Structure: glass/ITO/*a*-$TiO_x$/Active Layer/Au.

assuming no changes in materials properties, which again is contrary to what is observed. Following this same model, having a smaller shunt resistance (larger current under reverse bias) would also result in a smaller $V_{oc}$. However, the nanopatterned devices have a smaller shunt resistance as well as a larger $V_{oc}$ when compared to the thin-film devices (Supporting Information, Figure S3). To explain these results, it was hypothesized that the change in $V_{oc}$ must be related to a change in the interface composition of the BHJ due to electrode geometry.

To investigate this, *a*-$TiO_x$/P3HT single heterojunction solar cells were constructed to determine if electrode geometry would affect the $V_{oc}$. If the surface of *a*-$TiO_x$ was altered during the nanopatterning process (i.e., from stamp contamination), it would be expected that a similar change in $V_{oc}$ would be observed for the $TiO_x$/P3HT cells. However, both the planar and nanopatterned *a*-$TiO_x$/P3HT cell had comparable values for the $V_{oc}$ (≈0.60 V) (Figure 2b), in agreement with results on calcined nanopatterned $TiO_2$/P3HT cells.[14] The nanopatterned devices exhibited a much larger current in the forward bias direction similar to the BHJ devices. Furthermore, the $J_{sc}$ was found to scale with electrode surface area, increasing from 0.1 mA cm$^{-2}$ to 0.6 mA cm$^{-2}$. These results demonstrate that when the organic active layer interface compositions are held constant, the $V_{oc}$ remains constant. Therefore, it can be inferred that the increase in $V_{oc}$ is likely the result of a change in concentration of PCBM at the *a*-$TiO_x$/BHJ interface due to electrode geometry.

It is generally accepted that the $V_{oc}$ for an organic solar cell is correlated to the difference between the highest occupied molecular orbital (HOMO) of the donor material and the LUMO of the acceptor material.[20] However, it has been shown that $V_{oc}$ decreases if the cathode work function is lower than the LUMO of the acceptor or the anode work function is higher than that of the HOMO of the donor.[21] Furthermore, shifts of the Fermi energy at organic–organic interfaces, leading to the formation of an interfacial dipole and thereby a shift in the relative molecular orbital positions, have been observed.[22] Others have shown that interfacial modifiers form a fixed dipole at an inorganic/organic interface and modify the $V_{oc}$ of planar $TiO_2$/P3HT solar cells.[23] Given these previous studies, it is likely that the formation of an interfacial dipole by either charge transfer or a fixed dipole between *a*-$TiO_x$ and PCBM results in an increase in the conduction band (CB) level of *a*-$TiO_x$, thus reducing the $V_{oc}$. Furthermore, it is plausible that there is a relatively weak dipole formed between P3HT and *a*-$TiO_x$ because of the large difference in energy between the LUMO of P3HT and CB of *a*-$TiO_x$, thus having little effect on the CB level of the *a*-$TiO_x$. Therefore, it is reasoned that the increase in $V_{oc}$ observed in the nanopatterned *a*-$TiO_x$/P3HT:PCBM devices is due to the increase in P3HT concentration at the *a*-$TiO_x$/P3HT:PCBM interface resulting in less dipolar character between the *a*-$TiO_x$ and PCBM. It is reasonable that infiltration of the P3HT:PCBM into the *a*-$TiO_x$ nanopores results in the segregation of the P3HT to the *a*-$TiO_x$ interface resulting in less electrical contact between the PCBM and *a*-$TiO_x$, which explains the differences in $V_{oc}$ between the nanopatterned and planar *a*-$TiO_x$/BHJ devices processed with heat and pressure.

To gain further understanding of how the interfacial character could be controlled with processing, P3HT:PCBM devices with flat and nanopatterned *a*-$TiO_x$ were characterized after processing the active layer using three different methods: as-cast, infiltration by heat, and infiltration by heat and pressure (**Figure 3**). In our studies, it was found that upon processing with heat and pressure, the $V_{oc}$ increased by 0.1 V (relative to the as-cast samples) regardless of electrode geometry. These findings support the argument that the $V_{oc}$ is reduced by a *a*-$TiO_x$/BHJ interface rich in PCBM; similar results were previously observed in the literature for inverted devices with a PCBM rich

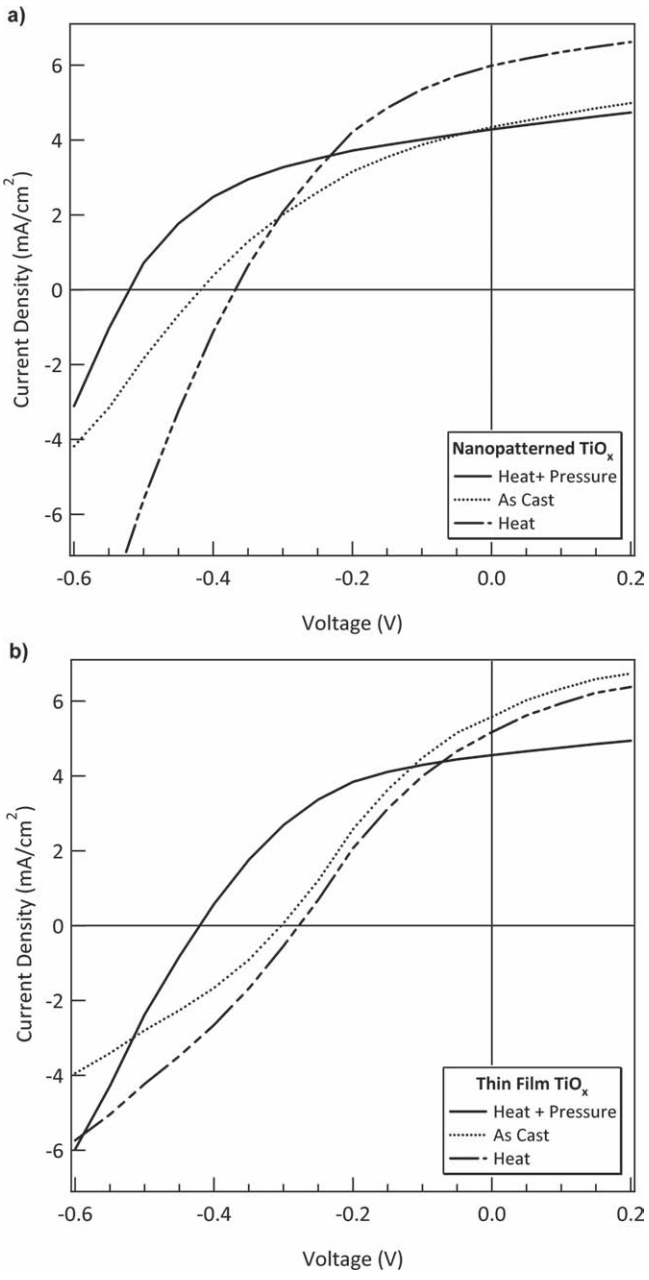


**Figure 3.** Current–voltage plots of a) nanopatterned and b) thin-film *a*-$TiO_x$/P3HT:PCBM devices. Structure: glass/ITO/ *a*-$TiO_x$/P3HT:PCBM/ Au.

layer at the oxide electrode.[24] The samples processed using heat and pressure are expected to have a lower concentration of PCBM at the *a*-$TiO_x$/active layer interface and thus a higher $V_{oc}$ because the contact of the soft stamp with the BHJ surface places an entropic penalty on the polymer at the BHJ/air interface by reducing the conformational entropy of the system.[25] This penalty sets up a driving force for the diffusion of PCBM to the top interface, thus depleting the PCBM at the *a*-$TiO_x$/BHJ interface resulting in the increase in $V_{oc}$. The increase in $V_{oc}$ observed between the as-cast planar and nanopatterned *a*-$TiO_x$/P3HT:PCBM devices is possibly due to flow of the material into the *a*-$TiO_x$ nanopattern during spin coating resulting in an interface with more P3HT character. However, it is difficult to differentiate between the contributions of flow and confinement to the $V_{oc}$ in the nanopatterned *a*-$TiO_x$/P3HT:PCBM and is reasonable that both contribute to the observed improvement in the $V_{oc}$.

It was also found that processing the nanopatterned and planar devices with just heat (without the gold electrode), decreased the average $V_{oc}$ relative to the as-cast devices (Figure 3). Continuing with the previous argument, a device processed with just heat provides a driving force for a P3HT rich BHJ/air interface because of an increase in conformational entropy of the polymer at the air interface. Furthermore, because the polymer is confined by the *a*-$TiO_x$ nanopattern, it is expected that the PCBM will diffuse to the *a*-$TiO_x$ interface allowing for an increase in conformation entropy of the polymer. The observed lowering of the $V_{oc}$ in both the nanopatterned and planar *a*-$TiO_x$/BHJ devices is consistent with this argument. It should be noted that only the entropy of the blend is considered and the enthalpic interactions of either components with the stamp or the *a*-$TiO_x$ interface are not accounted for. We also did not draw any conclusions from the change in $J_{sc}$ with processing because the changes were within the natural variation of the devices (see Supporting Information, Figure S5).

In conclusion, soft nonoimprint lithography can be used to form nanopatterned *a*-$TiO_x$ electrodes for inverted bulk heterojunction organic photovoltaics with improved device performance relative to planar layers. Surprisingly, the nanopatterned electrodes lead to an increase in $V_{oc}$ by 0.1 V. Application of heat and pressure was found to further increase the $V_{oc}$ by 0.1 V regardless of electrode geometry. It is likely that PCBM was depleted from the *a*-$TiO_x$/BHJ interface thus effectively lowering the conduction band of the *a*-$TiO_x$ resulting in an increase in $V_{oc}$. The key finding is that the $V_{oc}$ is sensitive to the composition of the BHJ/electrode interface and thereby, the infiltration method used to form OPVs with nanostructured electrodes.

## *Experimental Section*

*Stamp Fabrication*: The polymeric stamps based on PMMS were fabricated by the previously published procedure using ethoxylated (4) bisphenol A dimethacrylate and triallyl cyanurate as the crosslinkers.[14] The thiol-ene mixture was poured on a nanopatterned anodized alumina template that was pre-treated with a fluorinating agent. After curing, the stamps were peeled from the reusable template, and used without further treatment.

*Synthesis of Amorphous Titanium Suboxide (a-$TiO_x$)*: Titanium (IV) isopropoxide (0.4 mL) were added to a small vial charged with a stirring bar along with 0.08 mL of acetic acid. The solution was allowed to stir at room temperature for 30 min followed by the addition of 0.08 mL of hydrochloric acid and sequential stirring for an additional 10 min. Finally, 1.4 mL of *n*-butanol were added and allowed to stir for 10 min before use.

*Scanning Electron Microscopy*: Scanning electron microscopy (SEM) images were acquired using an FEI XL30 Sirion FEG digital electron scanning microscope. All cross-section samples were prepared by immersion in liquid nitrogen followed by fracture.

*Device Fabrication and Characterization*: ITO-coated glass substrates were ultrasonicated in acetone, 2% soap in water, deionized water, and 2-propanol for 20 min and dried with nitrogen. A 1:7 (sol-gel:butanol) solution was deposited at 4000 rpm for 45 s and cured in ambient

conditions at 140 °C for 10 min. The *a*-$TiO_x$ nanopatterns were fabricated by drop-casting the sol-gel on a glass/ITO/*a*-$TiO_x$ substrate, patterned with a PMMS stamp at 1 psi and 90 °C for 10 min, and further cured after peeling the stamp at 140 °C for 10 min in an ambient environment, followed by UV ozone treatment for 15 min. The P3HT:PCBM solution (1:0.7 by weight) with 2% vol 1,8-octanedithiol (97%) was prepared with the polymer concentration of 17 mg $mL^{-1}$ and stirred overnight at 110 °C. The solution was spin coated at varying rates between 700 and 1200 rpm for 60 s. In some cases, pressure (300 psi) was applied using a TDFOCS treated flat PMMS stamp.

A 100 nm thick Au anode was deposited by thermal evaporation under vacuum ($10^{-6}$ Torr). A part of the organic layer was removed to allow contact with the ITO, and then conductive Ag paste was painted to the area. Devices were measured at RT under argon with an Oriel xenon arc lamp and AM 1.5G solar filter. Current–voltage characteristics were recorded by a Keithley 236 SMU. The active area was 0.03 $cm^2$.

## Supporting Information

Supporting Information is available from the Wiley Online Library or from the author.

## Acknowledgements

The use of the central facilities of the UCSB Materials Research Laboratory (NSF Grant DMR05–20415) is gratefully acknowledged. Portions of this work were performed as a user project at the Molecular Foundry, at Lawrence Berkeley National Laboratory, which is supported by the Office of Science, Office of Basic Energy Sciences, of the U.S. Department of Energy under Contract No. DE-AC02 — 05CH11231. NDT acknowledges support from the ConvEne IGERT Program (NSF-DGE 0801627) and NSF Graduate Research Fellowship Program. LMC thanks the University of California for support with a President's Fellowship.

Received: May 28, 2010
Published online: September 8, 2010

[1] C. Waldauf, M. Morana, P. Denk, P. Schilinsky, K. Coakley, S. A. Choulis, C. J. Brabec, *Appl. Phys. Lett.* **2006**, *89*, 3517.
[2] H. H. Liao, L. M. Chen, Z. Xu, G. Li, Y. Yang, *Appl. Phys. Lett.* **2008**, *92*, 3303.
[3] K. Kawano, R. Pacios, D. Poplavskyy, J. Nelson, D. D. C. Bradley, J. R. Durrant, *Sol. Energy Mater. Sol. Cells* **2006**, *90*, 3520.
[4] C. S. Kim, S. S. Lee, E. D. Gomez, J. B. Kim, Y. L. Loo, *Appl. Phys. Lett.* **2009**, *94*, 3302.
[5] A. Shah, P. Torres, R. Tscharner, N. Wyrsch, H. Keppner, *Science* **1999**, *285*, 692.
[6] G. Dennler, M. C. Scharber, C. J. Brabec, *Adv. Mater.* **2009**, *21*, 1323.
[7] H. Y. Chen, J. H. Hou, S. Q. Zhang, Y. Y. Liang, G. W. Yang, Y. Yang, L. P. Yu, Y. Wu, G. Li, *Nat. Photonics* **2009**, *3*, 649.
[8] L. M. Campos, A. Tontcheva, S. Günes, G. Sonmez, H. Neugebauer, N. S. Sariciftci, F. Wudl, *Chem. Mater.* **2005**, *17*, 4031.
[9] A. C. Mayer, S. R. Scully, B. E. Hardin, M. W. Rowell, M. D. McGehee, *Mater. Today* **2007**, *10*, 28.
[10] C. G. Shuttle, B. O'Regan, A. M. Ballantyne, J. Nelson, D. D. C. Bradley, J. R. Durrant, *Phys. Rev. B: Condens. Matter.* **2008**, *78*, 113201.
[11] a) T. J. Savenije, J. M. Warman, A. Goossens, *Chem. Phys. Lett.* **1998**, *287*, 148; b) K. M. Coakley, M. D. McGehee, *Appl. Phys. Lett.* **2003**, *83*, 3380.
[12] a) W. J. E. Beek, L. H. Slooff, M. M. Wienk, J. M. Kroon, R. A. J. Janssen, *Adv. Funct. Mater.* **2005**, *15*, 1703; b) P. Ravirajan, A. M. Peiro, M. K. Nazeeruddin, M. Graetzel, D. D. C. Bradley, J. R. Durrant, J. Nelson, *J. Phys. Chem. B* **2006**, *110*, 7635.
[13] S. Cho, K. Lee, A. J. Heeger, *Adv. Mater.* **2009**, *21*, 1941.
[14] L. M. Campos, I. Meinel, R. G. Guino, M. Schierhorn, N. Gupta, G. D. Stucky, C. J. Hawker, *Adv. Mater.* **2008**, *20*, 3728.
[15] S. S. Williams, M. J. Hampton, V. Gowrishankar, I.-K. Ding, J. L. Templeton, E. T. Samulski, J. M. DeSimone, M. D. McGehee, *Chem. Mater.* **2008**, *20*, 5229.
[16] L. M. Campos, T. T. Truong, D. E. Shim, M. D. Dimitriou, D. Shir, I. Meinel, J. A. Gerbec, H. T. Hahn, J. A. Rogers, C. J. Hawker, *Chem. Mater.* **2009**, *21*, 5319.
[17] C. J. Brinker, G. W. Scherer, *J. Non-Cryst. Solids* **1985**, *70*, 301.
[18] a) R. Steim, S. A. Choulis, P. Schilinsky, C. J. Brabec, *Appl. Phys. Lett.* **2008**, 3303; b) S. Sista, M.-H. Park, Z. Hong, Y. Wu, J. Hou, W. L. Kwan, G. Li, Y. Yang, *Adv. Mater.* **2010**, *22*, 380.
[19] K. M. Coakley, B. S. Srinivasan, J. M. Ziebarth, C. Goh, Y. X. Liu, M. D. McGehee, *Adv. Funct. Mater.* **2005**, *15*, 1927.
[20] M. C. Scharber, D. Wuhlbacher, M. Koppe, P. Denk, C. Waldauf, A. J. Heeger, C. L. Brabec, *Adv. Mater.* **2006**, *18*, 789.
[21] V. D. Mihailetchi, P. W. M. Blom, J. C. Hummelen, M. T. Rispens, *J. Appl. Phys.* **2003**, *94*, 6849.
[22] H. Vazquez, W. Gao, F. Flores, A. Kahn, *Phys. Rev. B* **2005**, 71.
[23] C. Goh, S. R. Scully, M. D. McGehee, *J. Appl. Phys.* **2007**, 101.
[24] Z. Xu, L. M. Chen, G. W. Yang, C. H. Huang, J. H. Hou, Y. Wu, G. Li, C. S. Hsu, Y. Yang, *Adv. Funct. Mater.* **2009**, *19*, 1227.
[25] R. A. Vaia, E. P. Giannelis, *Macromolecules* **1997**, *30*, 7990.